TRAPPED PROTON MODELLING AT LOW ALTITUDE

D. Heynderickx, M. Kruglanski and J. Lemaire
BIRA-IASB, Ringlaan 3, B-1180 Brussel, Belgium

E.J. Daly
ESA/ESTEC, Postbus 299, NL-2200 AG Noordwijk, The Netherlands

Abstract The aim of the ESA-funded TREND (Trapped Radiation Environment Development) project is to evaluate and extend existing models of the Earth's trapped particle environment, and, where appropriate, to develop new models. At low altitude, protons interact with the atmosphere whose neutral density is a function of solar activity. Therefore the low-altitude cut-off of proton fluxes by atmospheric absorption is solar-activity dependent. The cut-off is a very important feature and explicit modelling of the geomagnetic-atmospheric control of particle fluxes is difficult. We report on work done for the low altitude region, including study of coordinate systems, tracing drift shells to deduce atmospheric control, and atmosphere-induced flux anisotropies. The construction of new a trapped proton model based on data from the AZUR particle telescopes is described. The new model is being included in the UNIRAD software package [*Heynderickx et al.*, 1996c].

Introduction

The description of the low-altitude part of the trapped radiation belts is complicated by the interaction of the Earth's atmosphere with the trapped particle population. In this paper, we highlight the various aspects of the interaction of the atmosphere with trapped protons and describe how they can be taken into account when building radiation belt models. This process is illustrated by means of the AZUR/88 [*Hovestadt et al.*, 1972] data set. A detailed description of the data processing for the AZUR instruments is given by *Heynderickx et al.* [1997].

The interaction of the atmosphere with the trapped proton population consists of three effects:

1. a sharp decrease of fluxes as a function of magnetic field intensity in the atmospheric loss cone;
2. an azimuthal dependence of the flux due to the scale height of the atmosphere which is of the same order as the gyroradii of energetic protons;
3. a dependence of the flux levels on the solar cycle through the response of the atmosphere to solar activity.

These effects will be discussed in the following sections, together with methods to account for them in empirical models.

Pitch angle dependence

It is well known that on a given field line the trapped proton flux decreases sharply with increasing magnetic field intensity B (or decreasing pitch angle α) in the altitude range where the atmosphere strongly interacts with the trapped particles. We illustrate this in Figure 1 with the dependence of the AZUR/88 channel 1 (1.5–2.7 MeV) differential proton flux on the equatorial pitch angle $\alpha_0 \equiv \arcsin(\sqrt{B_0/B}\sin\alpha)$, where $B_0 = 0.311653/L^3$.

Shell averaged atmospheric density

As a consequence of the steepness of the flux gradient, the determination of the flux in the atmospheric loss cone by interpolation in B, B/B_0 or α_0 strongly depends on the accuracy of the magnetic field representation. The situation may be improved by using, instead of a coordinate solely determined by the magnetic field distribution, a coordinate that depends on the atmospheric density distribution as well. *Heynderickx et al.* [1996b] proposed to use the atmospheric density, weighted with energy-dependent cross sections of the main interactions of the atmospheric constituents with energetic protons, averaged over the drift shell determined by the (B, L) coordinates of the trapped proton (we will use the notation n_s for this quantity). Using $\log n_s$ instead of B, B/B_0, or α_0, flattens out the flux dependence in the atmospheric loss cone: Figure 2 shows the dependence of the AZUR fluxes of Figure 1 in terms of n_s, where n_s was determined with the atmospheric model MSISE-90 and the magnetic field model GSFC 12/66 [*Cain et al.*, 1967], which was used by *Hovestadt et al.* [1972] to calculate (B, L) values for the AZUR mission.

The averaged flux in Figure 2 shows a nearly linear dependence on n_s, except for the highest values of n_s, which correspond to locations deep in the atmospheric loss cone. This linearity confirms the assumption made by *Lenchek and Singer* [1962] that the flux is inversely proportional to the atmospheric density averaged over an orbit.

ESA Symposium Proceedings on 'Environment Modelling for Space-based Applications', *ESTEC, Noordwijk, NL, 18-20 September 1996* (SP-392, December 1996)

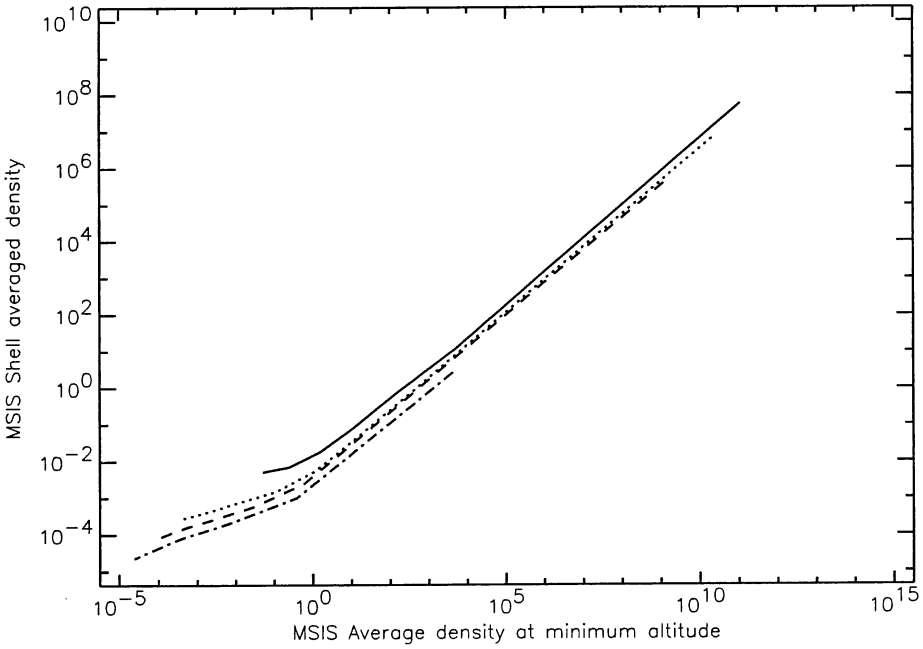

Figure 3. Comparison of n_s to $n_{h_{min}}$ calculated for a number of B values with four constant values of L: 1.2 (solid line), 1.5 (dotted line), 2.0 (dashed line), and 3.0 (dash-dot line).

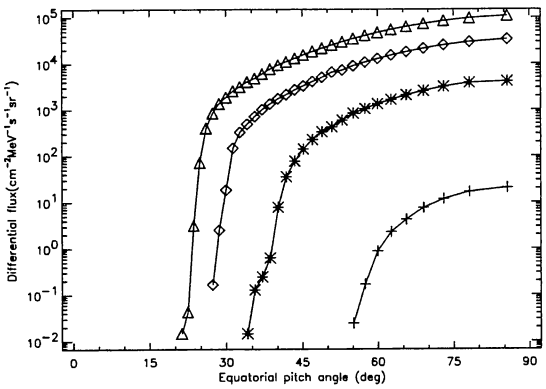

Figure 1. Equatorial pitch angle dependence of the AZUR/88 channel 1 proton flux (1.5–2.7 MeV) for four L values: 1.25 (+), 1.50 (*), 1.75 (◇), and 2.00 (△).

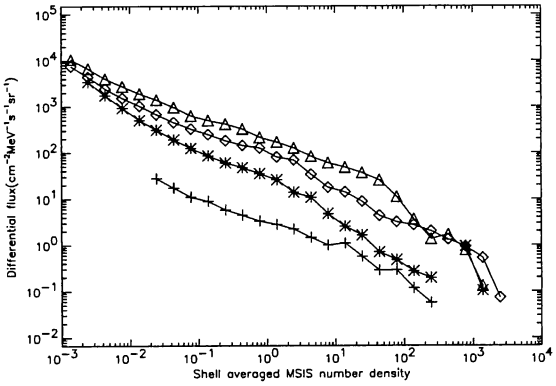

Figure 2. Dependence on the shell averaged atmospheric density of the AZUR/88 channel 1 proton flux (1.5–2.7 MeV) for four L values: 1.25 (+), 1.50 (*), 1.75 (◇), and 2.00 (△).

Alternative atmospheric density parameters

Although the parameter $\log n_s$ is better suited than B, B/B_0, or α_0 to represent the proton flux distribution at low altitudes, its calculation involves tracing a drift shell for each measurement, calculating the atmospheric density at a large number of points on the shell, and averaging the density over the shell. This process is very computation-intensive, even on modern fast work stations. In order to reduce the computation time, we have looked for alternative quantities to replace n_s.

As the atmospheric density increases nearly exponentially with decreasing altitude, the most significant contribution to the average in n_s is supplied by the intersection of the drift shell with the South Atlantic Anomaly (SAA) region, since this is the region where the trapped particles reach their minimum altitude. Figure 3 compares the shell averaged density n_s(MSISE-90) to the density at minimum altitude $n_{h_{min}}$(MSISE-90) for four L values. There appears to be a linear relation between $\log n_s$ and $\log n_{h_{min}}$, with different slopes for high and low density

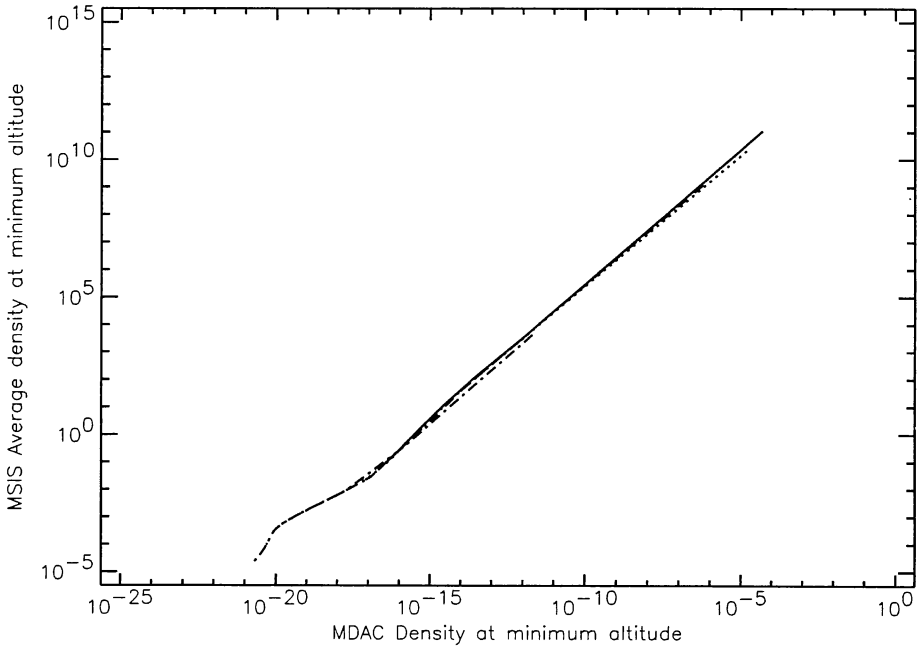

Figure 4. Comparison of $n_{h_{min}}$(MSIS) to $n_{h_{min}}$(MDAC) calculated for a number of B values with four constant values of L: 1.2 (solid line), 1.5 (dotted line), 2.0 (dashed line), and 3.0 (dash-dot line).

regions. This relation holds for L values up to 6, and for the intermediate L values not shown in Figure 3. The linear relation between $\log n_s$ and $\log n_{h_{min}}$ implies that the flux dependence on $\log n_s$ is equivalent to the dependence on $\log n_{h_{min}}$. This means in turn that in practice n_s can be replaced by $n_{h_{min}}$, thus eliminating the necessity of calculating the atmospheric density over the whole drift shell. However, it is still necessary to trace the drift shell, since the coordinates of the lowest-altitude point on the shell are needed.

There is a way to avoid the drift shell tracing as well: first, we found that n_s and $n_{h_{min}}$ do not depend significantly on the atmospheric density model. We have recalculated $n_{h_{min}}$ for the curves shown in Figure 3 with a simple atmosphere model developed by McDonnell Douglas Astronautics Co. (MDAC) [*Pfitzer*, 1990], that only depends on altitude and the solar radio flux $F_{10.7}$:

$$d = d_0 \exp\left(-\frac{z-120}{A\sqrt{z-103}}\right), \qquad (1)$$

where d is the mass density in $\mathrm{g\,cm^{-3}}$, $d_0 = 2.7 \times 10^{-11}\mathrm{g\,cm^{-3}}$, z is the altitude in km, and A is the solar cycle term:

$$A = 0.99 + 0.518\sqrt{\frac{F_{10.7} + F_{10.7A}}{110}}, \qquad (2)$$

with $F_{10.7A}$ the three-month average of $F_{10.7}$. The density d becomes infinite at $z = 103$ km, which corresponds to the rigid cutoff imposed by *Vette* [1991] for the AP-8 and AE-8 models.

In Figure 4, we compare the density at minimum altitude $n_{h_{min}}$(MSISE-90) to $n_{h_{min}}$(MDAC). Again, there is a linear relation between the logs of the densities, with three different slopes in different density regions. The relation appears to be independent of L. Consequently, the dependence of the fluxes on n_s(MSISE-90) or $n_{h_{min}}$(MSISE-90) does not differ significantly from the dependence on n_s(MDAC) or $n_{h_{min}}$(MDAC). While for the MSISE-90 model the three spatial coordinates of a point are needed, the altitude alone is sufficient for the MDAC model. This means that it is sufficient to know the lowest altitude h_{min} reached on a drift shell in order to calculate $n_{h_{min}}$(MDAC).

We then looked for a way to "predict" the lowest altitude reached on a drift shell from its (B, L) values. Figure 5 shows the minimum altitude h_{min}, calculated with our drift shell tracing library [*Heynderickx et al.*, 1996b], for a number of L values and a series of B/B_0 values, keeping L constant. It appears that h_{min} is a quadratic function of $\log(B/B_0)$, approaching a linear function for $L \lesssim 2$. The solid lines in Figure 5 represent the quadratic fits for the respective L values in the plot. Consequently, the minimum altitude on a drift shell (B, L) can be approximated by

$$h_{min} = \sum_{i=0}^{2} a_i(L) \left(\log \frac{B}{B_0}\right)^i \qquad (3)$$

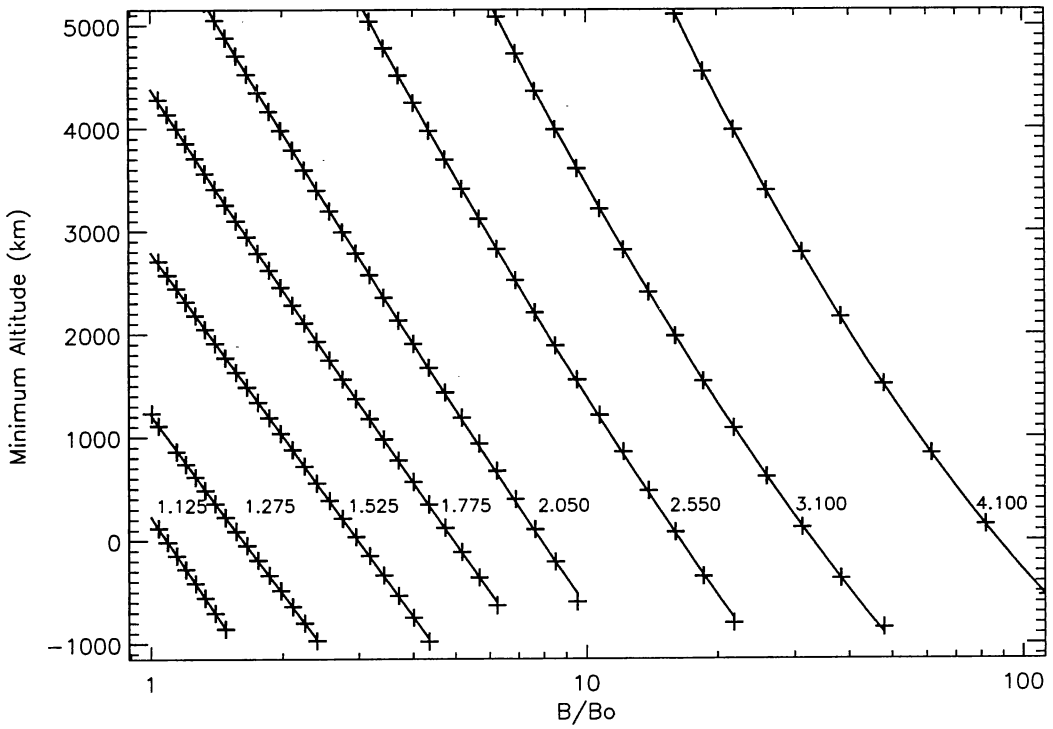

Figure 5. Minimum altitude on a set of drift shells defined by fixed L values (curve labels) and the B/B_0 values on the abscissa. The drift shell tracing was done with the GSFC 12/66 [*Cain et al.*, 1967] magnetic field model, updated to 1970. The solid lines are the parabolic fits defined in the text, for each L value.

to a high degree of accuracy. This means that, once the fit coefficients $a_i(L)$ have been determined for a sufficient number of L values—this has to be done only once for a given magnetic field model and epoch, the calculation of $n_{h_{min}}$ is reduced to deriving h_{min} with Eq. (3) and applying the resulting altitude to the MDAC model given by Eq. (1). In this way, the calculation of $n_{h_{min}}$ is greatly simplified, and it is now feasible to derive it for each measurement when averaging or binning satellite measurements.

Additional atmospheric effects

Solar cycle dependence

As the density distribution of the Earth's atmosphere depends on the solar activity cycle, the low-altitude trapped particle population varies during the solar cycle as well. The NASA AP-8 model [*Sawyer and Vette*, 1976] accounts for the solar cycle dependence only in a very basic way, i.e. it consists of two static versions, for solar minimum and solar maximum conditions, respectively.

The effect of the solar activity on the low-altitude trapped particle population is more subtle. Figure 6, taken from *Huston et al.* [1996], illustrates that the trapped proton flux increases gradually during the declining phase of the solar cycle, and decreases more rapidly during the ascending phase. The existence of a phase lag between the extrema of the trapped proton flux cycle and the extrema of the solar cycle is apparent as well.

The existence of different flux "regimes" for periods of low and high $F_{10.7}$ and the presence of a phase lag mean that the influence of the solar activity on the trapped particle population cannot be described by a simple linear correlation between $F_{10.7}$ and the particle flux. It is not clear yet what the exact relationship is, but it must involve a long-time history of the solar cycle activity.

Using $n_{h_{min}}$ as a parameter to order trapped particle fluxes should take into account the general trend of the particle flux behaviour in terms of $F_{10.7}$. A more accurate representation will necessarily involve an additional parameter related to the history of the solar cycle, such as the average of $F_{10.7}$ over several years or the phase of the solar cycle. It may prove to be necessary to make empirical models covering only sections of a solar cycle instead of one more general and comprehensive model. This approach would actually be beneficial in one aspect: due to the secular variation of the geomagnetic field, the

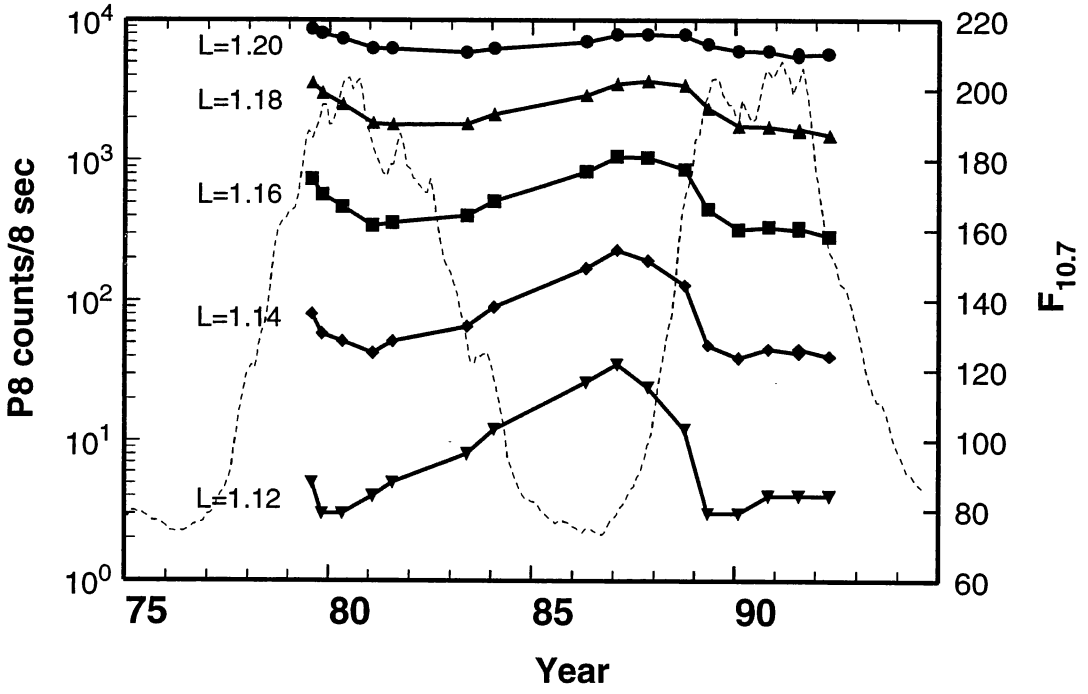

Figure 6. Variation of count rates in the 80–215 MeV channel of the TIROS/NOAA Space Environment Monitor (SEM) package over the solar cycle as a function of L. The dashed line shows the 13-month smoothed solar $F_{10.7}$ flux. (from *Huston et al.* [1996])

(B, L) coordinates are not conserved over time periods longer than a few years, so that over an 11-year period at least two sets of coordinates will have to be used.

Proton flux anisotropy

At low altitude, the interaction of trapped particles with the Earth's atmosphere induces, in addition to a pitch angle dependence, an azimuthal effect due to the finite size of the particles' gyration radius. This effect, which is observable when the gyroradii of the trapped protons become comparable with the atmospheric scale height, was first described by *Lenchek and Singer* [1962]. For a given point in space, trapped protons observed in different directions have their guiding centres on different magnetic field lines which belong to different drift shells. Therefore, during their drift motion, these particles traverse different amounts of atmospheric material and the flux observed in different directions will not be the same.

The density-related coordinates we described above only take into account the atmospheric density encountered by the guiding centre defined by the point of observation, and thus cannot account for directional effects. However, the coordinates n_s or $n_{h_{min}}$ can be combined with a function that provides the transformation from omnidirectional to directional flux in terms of the direction cosines and, for instance, (B, L) [*Kruglanski and Lemaire*, 1996].

Conclusions

We have discussed the main difficulties associated with modelling the low-altitude trapped proton population. We have shown how some of the features of the population can be modelled empirically and illustrated the solutions with the aid of AZUR data. The least understood aspect of the low-altitude proton population is the influence of the solar activity on the trapped particle flux. In order to better understand this important feature, long-duration missions (of the order of a solar cycle) with high-quality instruments are vital for establishing the necessary data bases. In addition, a better understanding of the CRAND effect would help in the theoretical modelling of the solar cycle effects.

Acknowledgements The AZUR data were obtained from NSSDC through Dr. J. King. We are greatly indebted to Dr. D. Hovestadt for his assistance in providing documentation and information on the AZUR data processing. This work was funded by ESA/ESTEC/WMA TRP Contract Nos. 9828/92/NL/FM and 10725/94/NL/JG(SC).

References

Cain J.C., S.J. Hendricks, R.A. Langel, and W.V. Hudson, A Proposed Model for the International Geomagnetic Reference Field-1965, *J. Geomag. Geoelec., 19*, 335–355, 1967.

Heynderickx, D., J. Lemaire, and E.J. Daly, Historical Review of the Different Procedures Used to Compute the *L*-Parameter, *Nucl. Tracks Radiat. Meas., 26*, 325–331, 1996a.

Heynderickx, D., M. Kruglanski, J.F. Lemaire, and E.J. Daly, A New Tool for Calculating Drift Shell Averaged Atmospheric Density, *Proc. Workshop on Radiation Belts: Models and standards, Brussels, 17–20 Oct., 1995*, ed. by J.F. Lemaire, D. Heynderickx, and D.N. Baker, AGU Monograph 97, 1996b.

Heynderickx, D., M. Kruglanski, J. Lemaire, D.J. Rodgers, A.D. Johnstone, R.H.W. Friedel, E. Keppler, G.D. Loidl, E.J. Daly, and H.D.R. Evans, New Features and Models in UNIRAD, this volume, 1996c.

Heynderickx, D., M. Kruglanski, and J. Lemaire, Flight Data Comparisons, Technical Note 5 for ESTEC Contract No. 10725/94/JG(SC), 1997.

Hovestadt, D., E. Achtermann, B. Ebel, B., Haüsler, and G., Pachmann, New observations of the proton population of the radiation belt between 1.5 and 104 MeV, Earth's Magnetospheric Processes, B.M. McCormac (ed.), D. Reidel Publishing Company, Dordrecht, Holland, 115–119, 1972.

S.L. Huston, G.A. Kuck, and K.A. Pfitzer, Low Altitude Trapped Radiation Model Using TIROS/NOAA Data, *Proc. Workshop on Radiation Belts: Models and standards, Brussels, 17–20 Oct., 1995*, ed. by J.F. Lemaire, D. Heynderickx, and D.N. Baker, AGU Monograph 97, 1996.

Kruglanski, M., and J. Lemaire, Trapped Proton Anisotropy at Low Altitudes, Technical Note 6 for ESTEC Contract No. 10725/94/JG(SC), 1996.

A.M. Lenchek, and S.F. Singer, Effects of Finite Gyroradii of Geomagnetically Trapped Protons, *J. Geophys. Res., 67*, 4073–4075, 1962.

Pfitzer, K.A., Radiation Dose to Man and Hardware as a Function of Atmospheric Density in the 28.5 Degree Space Station Orbit, MDSSC Report No. H5387 Rev A, 1990.

Sawyer, D.M., and J.I. Vette, AP-8 Trapped Proton Environment for Solar Maximum and Solar Minimum, NSSDC/WDC-A-R&S 76-06, 1976.

Vette, J.I., The NASA/National Space Science Data Center Trapped Radiation Environment Model Program (1964–1991), NSSDC/WDC-A-R&S 91-29, 1991.